



Intestinal basolateral lipid substrate transport is linked to chylomicron secretion and is regulated by apoC-III^S

Diana Li, Cayla N. Rodia, Zania K. Johnson, Minkyung Bae, Angelika Muter, Amy E. Heussinger, Nicholas Tambini, Austin M. Longo, Hongli Dong, Ji-Young Lee, and Alison B. Kohan¹

Department of Nutritional Sciences, University of Connecticut, Storrs, CT

Abstract Chylomicron metabolism is critical for determining plasma levels of triacylglycerols (TAGs) and cholesterol, both of which are risk factors for CVD. The rates of chylomicron secretion and remnant clearance are controlled by intracellular and extracellular factors, including apoC-III. We have previously shown that human apoC-III overexpression in mice (*apoC-III^{Tg}* mice) decreases the rate of chylomicron secretion into lymph, as well as the TAG composition in chylomicrons. We now find that this decrease in chylomicron secretion is not due to the intracellular effects of apoC-III, but instead that primary murine enteroids are capable of taking up TAG from TAG-rich lipoproteins (TRLs) on their basolateral surface; and via Seahorse analyses, we find that mitochondrial respiration is induced by basolateral TRLs. Furthermore, TAG uptake into the enterocyte is inhibited when excess apoC-III is present on TRLs. In vivo, we find that dietary TAG is diverted from the cytosolic lipid droplets and driven toward mitochondrial FA oxidation when plasma apoC-III is high (or when basolateral substrates are absent). We propose that this pathway of basolateral lipid substrate transport (BLST) plays a physiologically relevant role in the maintenance of dietary lipid absorption and chylomicron secretion. **Further, when apoC-III is in excess, it inhibits BLST and chylomicron secretion.**—Li, D., C. N. Rodia, Z. K. Johnson, M. Bae, A. Muter, A. E. Heussinger, N. Tambini, A. M. Longo, H. Dong, J.-Y. Lee, and A. B. Kohan. **Intestinal basolateral lipid substrate transport is linked to chylomicron secretion and is regulated by apoC-III.** *J. Lipid Res.* 2019. 60: 1503–1515.

Supplementary key words apolipoprotein C-III • low density lipoprotein receptor • enterocyte • dietary fat absorption • fatty acid oxidation • cytosolic lipid droplet • chylomicron

The intestine synthesizes a specialized lipoprotein, the chylomicron, containing both dietary triacylglycerol (TAG) and cholesterol, as well as apolipoprotein cargo. apoB-48

provides structure to the nascent chylomicron, while apoA-IV, apoA-I, and apoC-III function in the periphery to control plasma lipid metabolism and clearance, which directly controls the amount of lipopolysaccharide and oxidized lipids in circulation. Therefore, the intestine and its secreted chylomicrons are critical regulators of metabolic disease. Chylomicron overproduction is a common feature in patients with insulin resistance and obesity (1, 2) as well as in nondiabetic patients who have hyperlipidemia (3–5).

The regulation of chylomicron synthesis and secretion (including the transport of FFAs across the apical membrane, the enzymatic TAG reesterification pathway, and the construction and maturation of apoB-48-containing chylomicrons in the ER and Golgi) is driven by the presence of dietary fat in the small intestinal lumen. In response to rapid increases in apical lipid load after a meal, enterocytes rapidly incorporate dietary lipids into chylomicrons and use cytosolic lipid droplets (CLDs) as transient storage pools for dietary TAG. CLDs are dynamic organelles that play an active role in trafficking dietary lipid TAG between storage and chylomicron synthesis. CLD metabolism is driven by proteins located on the organelle's membrane, including perilipins (PLINs) (PLIN2 and PLIN3), TAG lipases (ATGL and HSL), and structural proteins (CIDEb) (6, 7).

Enterocytes are highly polarized epithelial cells, with dietary lipid absorption taking place at the apical membrane (facing the intestinal lumen) and chylomicron secretion occurring at the basolateral face into the intestinal lymph. The basolateral side of enterocytes faces both the vasculature and the intestinal lymphatics, providing access to circulating glucose, amino acids, and lipoproteins. It is becoming increasingly clear that plasma glucose and

This work was supported by National Institute of Diabetes and Digestive and Kidney Diseases Grant DK101663, U.S. Department of Agriculture Grant 11874590 (A.B.K.), and U.S. Department of Agriculture Hatch Formula Funds (Ascension #1017482 Project No. CONS00999) (A.B.K.). The content is solely the responsibility of the authors and does not necessarily represent the official views of the National Institutes of Health. The authors have no conflicts of interest to report.

Manuscript received 9 January 2019 and in revised form 31 May 2019.

Published, JLR Papers in Press, May 31, 2019

DOI <https://doi.org/10.1194/jlr.M092460>

Copyright © 2019 Li et al. Published under exclusive license by The American Society for Biochemistry and Molecular Biology, Inc.

This article is available online at <http://www.jlr.org>

Abbreviations: BLST, basolateral lipid substrate transport; CLD, cytosolic lipid droplet; FAO, FA oxidation; FCCP, fluoro-carbonyl cyanide phenylhydrazone; MAG, monoacylglycerol; OA, oleic acid; OCR, oxygen consumption rate; PGC1 α , peroxisome proliferator-activated receptor γ coactivator 1 α ; PLIN, perilipin; TAG, triacylglycerol; TEM, transmission electron microscopy; TICE, transintestinal cholesterol excretion; TRL, triacylglycerol-rich lipoprotein.

¹To whom correspondence should be addressed.

e-mail: alison.kohan@uconn.edu

S The online version of this article (available at <http://www.jlr.org>) contains a supplement.

amino acids regulate enterocyte energy metabolism and lipoprotein secretion (8–10), although the impact of lipoprotein uptake on enterocyte metabolism and lipoprotein secretion is unknown.

We have previously shown that apoC-III overexpression in mice decreases the rate of chylomicron secretion into lymph and results in the secretion of smaller chylomicrons that contain less TAG (11, 12). apoC-III is a major physiological inhibitor of LDLr and an independent risk factor for CVD (13, 14). Interestingly, the intestine has the second highest expression of *LDLR* next to the liver (15, 16), and LDLr is functionally active in the transport of LDL-cholesterol into the enterocyte (17).

In these studies, we measured the canonical intracellular chylomicron regulatory pathways (including chylomicron synthesis enzymes, FA trafficking across the apical membrane, and CLD metabolism). We also investigated whether enterocyte lipoprotein uptake regulates metabolism and dietary lipid absorption in order to better our understanding of how the pathophysiological conditions (like hyperlipidemia, diabetes, and inflammation) potentiate atherogenic chylomicron secretion. We determined that apoC-III acts in an extracellular manner to inhibit basolateral lipid substrate transport (BLST) into enterocytes, and this changes the activity of enterocyte mitochondria, CLDs, and chylomicron synthesis. We propose that the BLST pathway is an active regulator of chylomicron synthesis, and that the loss of BLST (in patients with pathophysiological apoC-III levels in plasma) could be atherogenic.

MATERIALS AND METHODS

Animals

Male and female C57BL/6 (WT), apoC-III transgenic (*apoC-III^{Tg}*), and apoC-III knockout (*apoC-III^{-/-}*) mice were used in the present study. *apoC-III^{Tg}* mice were bred in-house from heterozygous *apoC-III^{Tg}* founders. *apoC-III^{Tg}* mice were backcrossed six generations onto WT mice. *apoC-III^{Tg}* mice (founders generously provided by Dr. H. Dong, University of Pittsburgh) were originally generated by Dr. Jan Breslow and have been characterized extensively elsewhere (18, 19). Mice were aged from 8 to 24 weeks for all studies. Animals were maintained on a 12 h light-dark cycle at $21 \pm 1^\circ\text{C}$. All mice had ad libitum access to water and chow diet (LM-485 mouse/rat sterilizable diet; Harlan Laboratories). All animal procedures were performed in accordance with the University of Connecticut Institutional Animal Care and Use Committee and in compliance with the National Institutes of Health *Guide for the Care and Use of Laboratory Animals*.

Cardiac perfusion and transmission electron microscopy

Jejuna from gavaged mice were fixed and collected for transmission electron microscopy (TEM) imaging as previously described (6). Mice were fasted overnight and then given an oral gavage of 200 μl of olive oil. Two hours after gavage, the mice were anesthetized using inhaled isoflurane and perfused with 1.5% glutaraldehyde in 0.1 M sodium cacodylate via cardiac infusion. After fixation, tissue from the jejunum was isolated, stained with osmium tetroxide, dehydrated, and embedded in resin. Ultrathin sections were stained with lead citrate and uranyl acetate and examined.

Quantification of CLDs

Biological replicates ($n = 3$) were quantified with technical replicates ($n = 6$; six enterocytes from each mouse). The diameters of CLDs were measured using Fiji software (ImageJ). We considered the CLDs as 0.25–6.0 μm in diameter. The average diameter of CLDs was calculated on a per cell basis.

The surface areas of the CLDs were calculated by using the equation $\pi \times r^2$, where π is the value pi and r is the radius. The diameters of ellipsoid-shaped CLDs were measured across the point of the circle that represented the average diameter of that circle (avoiding the shortest and longest diameter).

Total TAG content of intestinal tissue

Lipids were extracted according to Folch, Lees, and Sloane (20). In brief, equal amounts of proximal intestinal tissue were homogenized in 2 ml of DPBS in a glass 15 ml conical tube, resuspended in 2 ml of 2:1 chloroform:methanol, and mixed by shaking for 2 min. Two milliliters of DEPC-treated water were then added, and samples were centrifuged for 30 min at 350 g . The aqueous and impurity phase was removed, and sodium sulfate was added to remove any residual moisture. The sample was then spun for 2 min at 350 g . The organic solvent supernatant was recovered and dried under a stream of nitrogen, and the lipids were resuspended in 0.1 M Triton X-100 and used for TAG assays using the GPO-PAP method (Radox TAG assay; Radox Laboratories, UK).

Lipid droplet isolation

CLDs were isolated from the intestinal mucosa of mice 4 h post-gavage according to a previously published protocol (21). Tissues were homogenized on ice in 0.8 ml of PBS supplemented with 5 mM EDTA and protease inhibitors (HALTTM protease inhibitor cocktail, #78430; Thermo Scientific) and centrifuged at 250 g at 4°C for 10 min to eliminate tissue debris. The remaining supernatant was named “I” for intestinal homogenate and was used to isolate three distinct CLD fractions by differential ultracentrifugation (TLA 110; Beckman Coulter). The first fraction (D1) was isolated after centrifugation at 20,000 g for 30 min at the surface of a top cushion of PBS ($d = 1 \text{ g/ml}$) and was referred to as large. Medium-sized droplets, referred as fraction D2, were then isolated after ultracentrifugation at 100,000 g for 1 h at $d = 1 \text{ g/ml}$. The remaining infranatant was adjusted to $d = 1.21 \text{ g/ml}$ with KBr, overlaid by a cushion of phosphate buffer at the same density, and ultracentrifuged for 14 h at 120,000 g and 4°C . The top fraction (D3) was recovered and referred to as small. Total lipid was extracted from CLD fractions by Folch extraction, resuspended in 0.1 M Triton X-100, and used for TAG assays.

Isolation of epithelial cells for flow cytometry

The intestines were excised from anesthetized mice and washed with cold PBS and then cut into 5 mm pieces. Intestine pieces were incubated in chelation buffer containing 2 mM EDTA in PBS for 30 min at 37°C with intermittent shaking every 10 min. Epithelial cells were collected by straining the sample through a 70 μm cell strainer to separate the single cells from the tissue pieces. Epithelial cells were then used for flow cytometry preparation.

Flow cytometry

Cells were stained with a live/dead discrimination dye (Zombie UV, #423107; Biolegend). Samples were stained with anti-mouse fluorochrome-conjugated antibodies for surface markers (EpCAM) and cell-permeant chemicals (HCS Lipid Tox, MitoSpy Green and Red). All antibody staining was conducted on ice and protected from light. Samples were fixed in 2% paraformaldehyde.

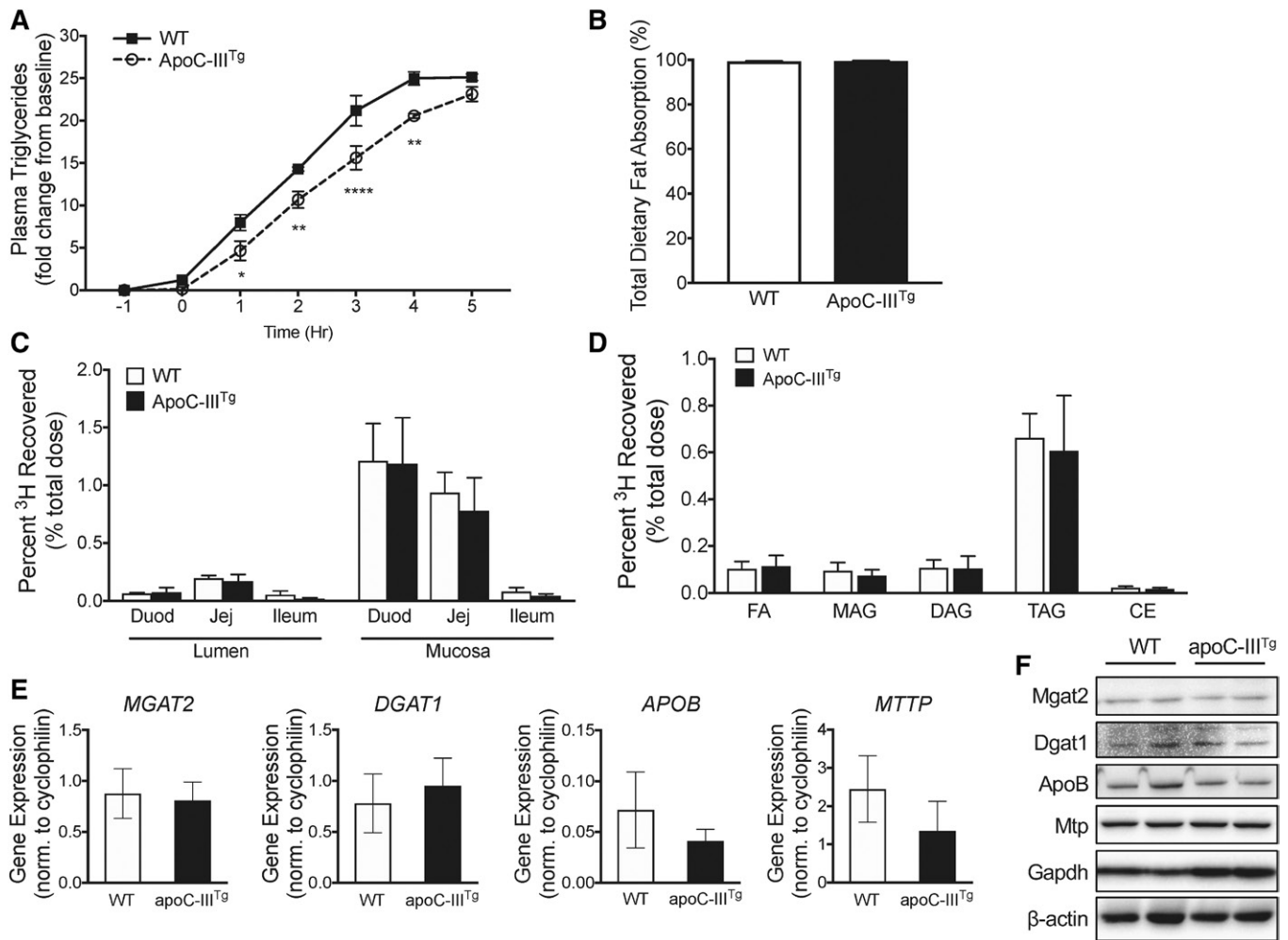


Fig. 1. apoC-III overexpression inhibits chylomicron secretion without changing the expression of chylomicron synthesis and secretion machinery. **A:** Chylomicron secretion measured by change in plasma TAGs after an injection of poloxamer 407 30 min prior to an olive oil gavage (time = 0 h). **B:** Percent total dietary lipid absorption measured using sucrose polybehenic acid tracer. **C:** Percent ^3H recovered in lumen and mucosa of duodenum, jejunum, and ileum 3 h post-gavage of ^3H -OA in olive oil. **D:** Percent tritium (^3H) recovered of various lipid species in jejunum mucosa 3 h post-gavage. **E, F:** mRNA (**E**) and protein (**F**) expression of TAG synthesis enzymes (MGAT2 and DGAT1) and chylomicron synthesis proteins (APOB and MTTP) in intestine. In all panels, error bars indicate SEM. In all studies, $n = 3\text{--}5$ for all genotypes, with experiments repeated at least twice. For **A**, statistical significance and interaction between genotypes was determined using two-way ANOVA with Sidak's post hoc analysis ($*P < 0.05$, $**P < 0.01$, $****P < 0.0001$).

Cells were washed between each step using flow cytometry buffer ($1\times$ PBS, 5% fetal bovine serum, 0.2 mM EDTA). Flow cytometry samples were run at the University of Connecticut Health Center Flow Cytometry Core.

Samples were run using the BD LSR II (Becton-Dickinson Biosciences) after appropriate compensation. Collected events were set at 100,000. Compensation controls using single stains were made using OneComp ebeads and UltraComp ebeads (Ebioscience) according to manufacturer's instructions.

Automatic compensation was conducted by FACs Diva software. Fluorescence minus one controls were used to determine appropriate gate positions. Detailed gating strategies, including sample fluorescence minus one gating strategies, are shown in supplemental Fig. S2. FlowJo software (Treestar, Ashland, OR) was utilized for final analysis of collected data. For absolute cell numbers, the percentage of living cells of a certain subset was multiplied by the number of living cells as determined by TC20 automated cell counter (Bio-Rad Laboratories, Inc., Hercules, CA). A list of the antibodies and stains used for flow cytometry are provided in supplemental Table S1.

Seahorse XF analyzer measurements of 3D enteroids

The 3D enteroids were cultured based on a previous protocol (12, 22). Biological replicates ($n = 3$) were used with technical replicates ($n = 3$; three wells on each cell culture plate), and the assay was run over the course of three different days. Real-time oxygen consumption rate (OCR) and extracellular acidification rate were determined by using an XF-24 extracellular flux analyzer (Seahorse Bioscience). Enteroids were cultured in Matrigel until maturity and then disassociated from the Matrigel and resuspended in medium containing rho-kinase inhibitor. Enteroids were treated with TAG-rich lipoproteins (TRLs) containing 400 μM TAG on the basolateral face of enteroids for 2 h prior to the assay being run. TRLs containing low apoC-III content [designated TRLs (low apoC-III)] were isolated from WT mice, while TRLs containing high apoC-III content [designated TRLs (high apoC-III)] were isolated from *apoC-III*^{Tg} mice. Enteroids were washed with assay medium three times to remove excess TRLs. A total of 3,000 enteroids were seeded per well. After attachment, cells were treated for the indicated times with inhibitors. The assay was performed in triplicate measurements in DMEM-based

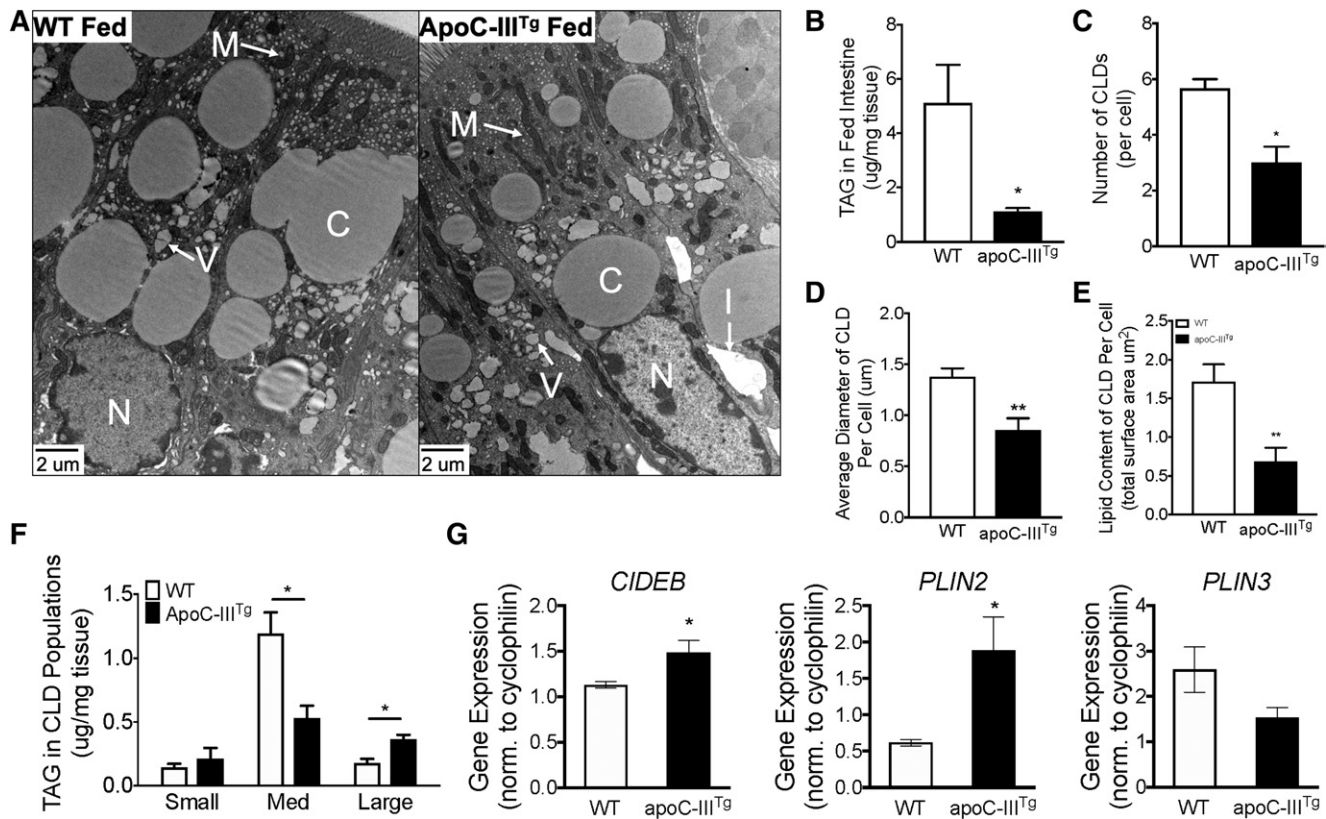


Fig. 2. *apoC-III^{Tg}* enterocytes have smaller CLDs with less TAG during dietary lipid absorption. A: TEM micrographs of jejunum enterocytes collected from WT and *apoC-III^{Tg}* mice 2 h post-gavage (C, CLDs; N, nucleus; M, mitochondria; I, interstitial space; V, vesicles containing lipid) (52, 53). B: TAG content (micrograms) in fed intestinal tissue normalized to tissue weight (milligrams) ($n = 4-7$ per genotype). C: Number of CLDs in WT and *apoC-III^{Tg}* enterocytes that are greater than 1 μm in diameter quantified from TEM micrographs. D: Average diameter of CLDs per enterocyte quantified from TEM micrographs. E: Lipid content expressed as total CLD surface area in WT and *apoC-III^{Tg}* enterocytes quantified from TEM micrographs. F: TAG content normalized to tissue weight of small, medium, and large CLDs purified from fed intestinal tissue using ultracentrifugation. G: mRNA expression of key proteins involved in CLD structure in fed intestine. In all panels, error bars indicate SEM. Biological replicates ($n = 3$) were analyzed by TEM (and at least six different enterocytes along the same crypt villus axis of each experimental animal were analyzed). Statistical significance and interaction between genotypes were determined by two-tailed Student's *t*-test (* $P < 0.05$, ** $P < 0.01$).

medium without bicarbonate supplemented with 5.5 mM glucose and 2 mM glutamine. Three consecutive measurements were performed under basal conditions and after the sequential addition of 1 μM of oligomycin, 1 μM of fluoro-carbonyl cyanide phenylhydrazone (FCCP), 2.5 μM of rotenone, and 2.5 μM of antimycin. All reagents were purchased from Sigma.

Dil-VLDL uptake by 3D enteroids

The 3D WT mouse enteroids were cultured based on a previous protocol (12, 22). Enteroids were collected from Matrigel and resuspended in medium that contained rho-kinase inhibitor. Enteroids were incubated at 37°C in a CO₂ incubator for 6 h with 5 $\mu\text{g}/\text{ml}$ of human Dil-VLDL (Kalen Biomedical, Germantown, MD) that contained physiological concentrations ($1\times = 0.143 \text{ mg}/\text{ml}$) of apoC-III, 2 \times , and 4 \times the physiological concentration of apoC-III (23, 24). Additional recombinant human apoC-III protein (Academy Bio-Medical, Houston, TX) was vortexed onto Dil-VLDL particles for 2 \times and 4 \times treatments. Enteroids were collected and cellular Dil fluorescence was analyzed by flow cytometry using the PE channel with unstained control and purity check.

Dietary FA secretion assay in 3D enteroids

Matrigel was removed from mature WT 3D enteroids, and cells were incubated at 37°C in medium containing Y27623 Rho-kinase inhibitor for 16 h. For treatment with TRLs without

apoC-III (–apoC-III), TRLs were isolated from apoC-III knock-out mice. For treatment with TRLs with excess apoC-III (+apoC-III), TRLs were isolated from *apoC-III^{Tg}* mice. TRLs were added to the medium (to be delivered on the basolateral face of the enteroids) at 100 and 400 μM final concentrations. After the 16 h incubation, 3D enteroids were opened by gentle pipetting and then treated with lipid micelles [0.6 mM of oleic acid (OA), 2 mM of taurocholate, 0.2 mM of 2-palmitoylglycerol, 0.05 mM of cholesterol, and 0.2 mM of phosphatidylcholine] and 1 μCi of ³H-OA for 1 h. Cells were then washed three times with PBS at 2.2 g for 2 min. Chase medium was then added to the enteroids, and cells were incubated for 3 h at 37°C to allow for chylomicron secretion. Cells were spun down and medium was collected for scintillation counting. The cell pellet was collected in RIPA buffer for a BCA protein assay in order to normalize counts by total protein.

Culture of 2D enteroids on Transwells

The 2D enteroids were grown using a protocol adapted from Wang et al. (25). Crypts were isolated from WT mice and seeded onto collagen hydrogel in 6-well Transwell cell culture plates.

Experiments were conducted on confluent cells [i.e., when transepithelial electrical resistance was greater than 400 $\Omega\text{-cm}^2$] (26). Cells were collected after collagenase (type IV, Worthington Biochemical LS004189; Lakewood, NJ) treatment.

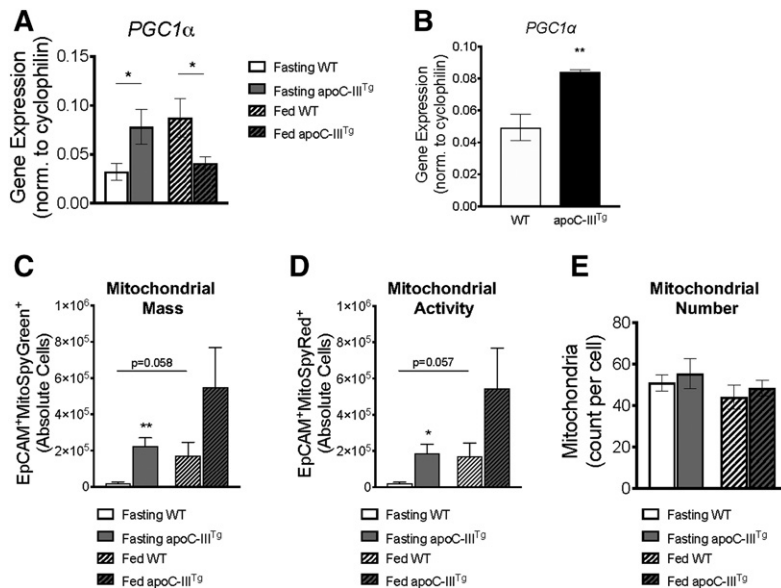


Fig. 3. *apoC-III^{Tg}* enterocytes have greater mitochondrial mass and activity in vivo. mRNA expression of *PGC1α* in fasted and fed intestine (A) and in fasted primary intestinal epithelial cells (B). C: Mitochondrial content (MitoSpy GreenTM) per intestinal epithelial cell in fasted and fed conditions in WT and *apoC-III^{Tg}* mice measured by flow cytometry. D: Mitochondrial activity (MitoSpy RedTM) per intestinal epithelial cell in fasted and fed conditions in WT and *apoC-III^{Tg}* mice. E: Mitochondrial number in fasted and fed enterocytes counted in TEM micrographs. In all panels, error bars indicate SEM [n = 4–8 in all studies except TEM, where n = 3 biological replicates were analyzed (and at least six technical replicates per animal)]. Statistical significance and interaction between genotypes were determined by two-tailed Student's *t* test (**P* < 0.05, ***P* < 0.01).

FA oxidation assay with 2D enteroids

FA oxidation (FAO) in 2D WT enteroids was measured using a ¹⁴C-OA (American Radiolabeled Chemicals Inc., St. Louis, MO) tracer using a previously published protocol (27). We measured FAO in untreated (control) and treated (with the addition of TRLs) 2D WT enteroids.

Briefly, cells were plated on 6-well Transwell plates and grown to confluency (see previously described protocol). The medium was changed to DMEM with 1.5% BSA, 0.1 mM OA, and ¹⁴C-OA (1 μCi/ml), and cells were incubated with the labeled medium for 16 h. Labeled medium was collected at the end of the incubation and chase medium containing DMEM with 1.5% BSA was added. Cells were incubated with chase medium for 4 h, after which the medium was collected in 25 ml airtight Erlenmeyer flasks for FAO measurement. Lipid oxidation was stopped with the addition of 200 μl of 70% perchloric acid to the bottom of the flask, driving the bicarbonate into CO₂. ¹⁴CO₂ was captured on a piece of KOH-soaked filter paper. After incubating the filter paper in the flask for 1 h at room temperature, the filter paper was analyzed for ¹⁴C activity by liquid scintillation counting of ¹⁴CO₂. Total protein was recovered by solubilizing the cells in 1× RIPA buffer and measured using a BCA assay (Pierce, Thermo Fisher Scientific). ¹⁴CO₂ counts were then normalized to the total dose and total cell protein.

A diagram of the treatment conditions is shown in Fig. 8C.

Collection of luminal contents and mucosal tissue

Mice were gavaged with ³H-OA (American Radiolabeled Chemicals; #ART 0198) in olive oil. At 1 and 3 h post-gavage, mice were euthanized with isoflurane and cervical dislocation. Both ends of the stomach, small intestine, and colon were tied with sutures to prevent leakage of the luminal contents. The small intestine was carefully further divided into three equal-length segments (labeled 1–3) corresponding to the proximal and distal ends. The luminal contents of the three segments were collected by washing three times with 1 ml of 10 mmol/l sodium taurocholate. The luminal content aliquots were taken for determination of radioactivity. The three small intestinal segments were cut open longitudinally and placed flat on a glass plate (luminal side up), and the mucosa was scraped with a glass slide. The lipid in both the lumen and mucosa was extracted by the Folch method (20). Radioactivity in aliquots of extracted lipid from luminal contents and mucosal

tissue were determined by liquid scintillation counting. The amount of triolein remaining in the lumen or mucosa at the end of the experiment was calculated as a percentage of the total counts per minute of radioactive OA gavaged.

TLC

Total lipid extracted through the Folch method was solubilized in 2:1 v/v CHCl₃:methanol and loaded onto activated silica gel G plates, and the lipids were fractionated using a solvent system of petroleum ether/diethyl ether/glacial acetic acid with a 25:5:1 vol ratio. Iodine vapor was used to visualize the different lipid classes as well as the comigrating lipid standards. The spots corresponding to TAG, diacylglycerol, monoacylglycerol (MAG), FFA, and phospholipid were scraped into scintillation vials containing Opti-Fluor scintillation fluid (Perkin Elmer, Hebron, KY) for scintillation counting the following day.

Total dietary fat absorption

The SPB method was developed and validated by Jandacek, Heubi, and Tso (28). It is a noninvasive method for studying the uptake of FA. The animals are fed a diet containing TAG and other essential nutrients. The method relies on measuring the ratio of fecal FAs versus fecal nonabsorbable fat marker. In this study, the uptake of total dietary FA (mass) was measured against the nonabsorbable lipophilic marker, sucrose polybehenate.

TRL isolation

Mice were fasted for 12 h and then gavaged with 200 μl of olive oil. Blood was collected through cardiac puncture at 3 h post-gavage. Serum was isolated and transferred to ultracentrifuge tubes (#342412; Beckman Coulter, Brea, CA), and 300 μl of sterile saline (0.15 M NaCl, d = 8.7 g/ml) was overlaid on top of the serum followed by ultracentrifugation at 41,160 *g* in a TLA110 rotor (Beckman Coulter) for 16 h at 4°C. TRLs were isolated from the top layer after ultracentrifugation.

Oral lipid tolerance test

Mice were fasted for 12 h, and then Poloxamer 407 (1 mg/g body weight) was intraperitoneally injected to block LPL activity. Mice were gavaged with a bolus of olive oil 30 min after Poloxamer 407 injection. Plasma was collected over the course of 6 h, and

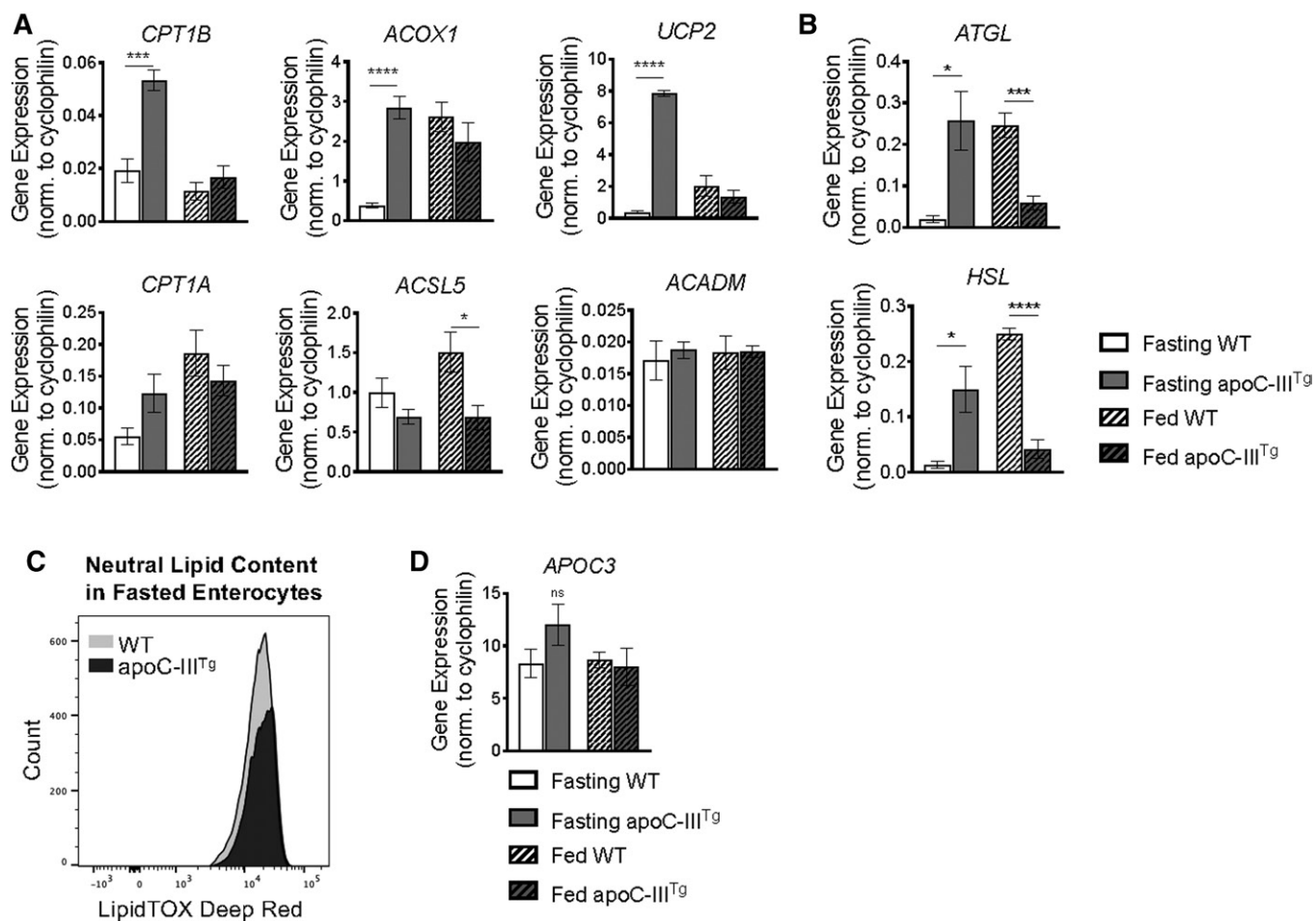


Fig. 4. FAO and TAG lipase gene expression is higher in *apoC-III^{Tg}* intestine during fasting. A: mRNA expression of key proteins involved in FAO in fasted and fed intestine of WT and *apoC-III^{Tg}* mice. B: mRNA expression of TAG lipases in fasted and fed intestine of WT and *apoC-III^{Tg}* mice. C: Total neutral lipid (LipidTox Deep Red™) per intestinal epithelial cell in fasting conditions in WT and *apoC-III^{Tg}* mice. D: mRNA expression of mouse *APOC3* in fasted and fed intestine. In all panels, error bars indicate SEM [n = 4–8 in all studies except TEM, where n = 3 biological replicates were analyzed (and at least six technical replicates per animal)]. Statistical significance and interaction between genotypes were determined by two-tailed Student's *t*-test (**P* < 0.05, ****P* < 0.001, *****P* < 0.0001).

TAG content in plasma was measured using a TAG assay to determine the rate of dietary fat absorption.

Statistics

Overall statistical significance was determined by two-tailed unpaired *t*-tests, unless otherwise noted; differences were considered significant at *P* < 0.05. All data are presented as mean ± SEM. Statistics were performed using GraphPad Prism (version 7.0)

RESULTS

apoC-III overexpression inhibits chylomicron secretion without changing the expression of chylomicron synthesis and secretion machinery

We previously showed that *apoC-III^{Tg}* mice secrete less dietary TAG into the lymph and secrete smaller chylomicron particles (11, 12). Using an oral lipid tolerance test in WT and *apoC-III^{Tg}* mice, we confirmed that the appearance of TAG in plasma occurs at a slower rate in *apoC-III^{Tg}* mice compared with their WT counterparts (Fig. 1A). This defect in chylomicron secretion is not associated with a defect in total dietary lipid absorption (Fig. 1B) measured by

quantifying the amount of the nonabsorbable polybehenic acid tracer in feces (28). We also tracked lipid absorption throughout the small intestine using an olive oil gavage containing ³H-OA, and we found no regional differences in mucosal lipid absorption between WT and *apoC-III^{Tg}* mice (Fig. 1C).

Dietary TAG is hydrolyzed in the intestinal lumen to MAG and FFAs. MAG and FFAs are absorbed into the enterocyte through protein transporters and passive diffusion at the apical membrane, followed by rapid resynthesis into TAG. MGAT2 and DGAT1 synthesize TAG at the ER membrane. We investigated the ability of *apoC-III^{Tg}* mice to incorporate ³H-OA into ³H-TAG in the intestinal mucosa by separating the different mucosal lipid species via TLC after oil gavage. We found that *apoC-III^{Tg}* mice incorporate dietary ³H-OA into ³H-TAG at a similar rate to WT mice (Fig. 1D). We next investigated mRNA and protein expression of the chylomicron synthetic machinery. We found no changes in expression of MGAT2, DGAT1, APOB, or MTTP in *apoC-III^{Tg}* mice compared with WT mice (Fig. 1E, F). We conclude that there are no changes in total dietary lipid absorption, regional lipid absorption, or any defects

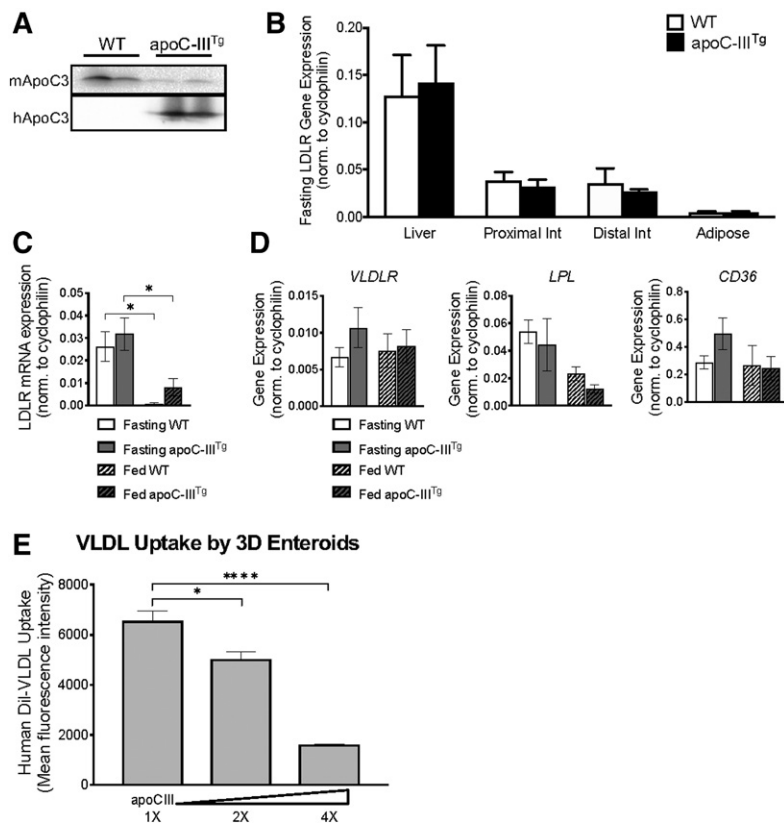


Fig. 5. High levels of plasma apoC-III inhibit intestinal uptake of TRLs. A: Protein expression of mouse and human apoC-III in plasma of WT and *apoC-III^{Tg}* mice. B: mRNA expression of *LDLR* measured in whole tissue homogenates of liver, proximal small intestine, distal small intestine, and epididymal adipose of fasting WT and *apoC-III^{Tg}* mice. C: mRNA expression of *LDLR* in fasted and fed intestine. D: mRNA expression of key transporters (*VLDLR* and *CD36*) and enzymes (*LPL*) involved in lipid uptake in fasted and fed intestine. E: Human DiI-VLDL uptake by WT mouse enteroids containing physiological concentrations of apoC-III (1×), 2×, and 4× the physiological concentration of apoC-III. Statistical significance was determined using a one-way ANOVA with Bonferroni post hoc analysis (* $P < 0.05$, **** $P < 0.0001$). In all panels, error bars indicate SEM. In all studies, $n = 3-5$ for all genotypes except for enteroid studies where $n = 5$. Statistical significance and interaction between genotypes were determined by two-tailed Student's *t*-test (* $P < 0.05$) unless otherwise indicated.

in TAG re-esterification or the chylomicron synthetic machinery in *apoC-III^{Tg}* mice that can explain the defect in chylomicron secretion.

CLDs are dramatically reduced in *apoC-III^{Tg}* enterocytes

Enterocytes utilize CLDs to store large quantities of neutral lipid during dietary lipid absorption. The temporary storage of dietary TAG in CLDs is necessary to facilitate highly efficient dietary lipid absorption while avoiding ER stress caused by lipid overload. Ablation of key proteins involved in CLD metabolism leads to the accumulation of dietary lipid in CLDs and defective chylomicron secretion (29–32). We hypothesized that *apoC-III^{Tg}* enterocytes have defects in either CLD storage or increased mitochondrial respiration that might explain the defect in chylomicron and dietary TAG secretion. We evaluated enterocyte CLD morphology via TEM imaging of jejunal enterocytes after an olive oil gavage (Fig. 2A). We found that the *apoC-III^{Tg}* intestinal mucosa contains less TAG and significantly fewer CLDs (Fig. 2B, C). Furthermore, *apoC-III^{Tg}* enterocytes have smaller CLDs (Fig. 2D). By analyzing the surface area of the CLDs (6), we find that the CLDs from *apoC-III^{Tg}* enterocytes contain less lipid (Fig. 2E). Using a biochemical approach, CLDs were purified from fresh tissue by density and size, and TAG content in the individual fractions of CLDs was measured via Folch extraction and biochemical TAG assay (21). We found significant changes in the distribution of TAG between the different fractions of *apoC-III^{Tg}* CLDs (Fig. 2F). Additionally, we measured mRNA expression for CLD structural proteins (*CIDEB*) and metabolic regulatory proteins (*PLIN2* and *PLIN3*) in fed intestine.

CIDEB and *PLIN2* play an important role in the stabilization of CLD TAG (33, 34). Both *CIDEB* and *PLIN2* mRNA are increased in the fed *apoC-III^{Tg}* intestine (Fig. 2G), which suggests that remodeling of the CLDs in *apoC-III^{Tg}* mice is occurring. We conclude that *apoC-III^{Tg}* enterocytes have significantly altered CLD metabolism that results in decreased CLD lipid storage that occurs concurrently with a decrease in dietary TAG secretion.

apoC-III^{Tg} enterocytes have greater mitochondrial mass and activity in vivo

We next investigated whether *apoC-III^{Tg}* enterocytes undergo increased FAO that might explain the loss of TAG content in CLDs and chylomicrons. Peroxisome proliferator-activated receptor γ coactivator 1 α (*PGC1 α*) is the master regulator of mitochondria (35). During fasted conditions, *apoC-III^{Tg}* intestine has significantly higher *PGC1 α* mRNA expression compared with WT (Fig. 3A), and this was confirmed in fasting primary enterocytes (Fig. 3B). Because *PGC1 α* upregulates mitochondrial biogenesis (36), we measured in vivo mitochondrial mass and activity in WT and *apoC-III^{Tg}* primary enterocytes using MitoSpy GreenTM and MitoSpy RedTM, respectively. We found that *apoC-III^{Tg}* enterocytes have increased MitoSpy GreenTM and MitoSpy RedTM staining compared with WT (Fig. 3C, D). The increase in mitochondrial mass and activity does not correlate with an overall increase in the total number of mitochondria in WT and *apoC-III^{Tg}* enterocytes (quantified via TEM in Fig. 3E, with TEM images shown in supplemental Fig. S3). This suggests that the individual mitochondria in *apoC-III^{Tg}* enterocytes are larger and more active than WT mitochondria.

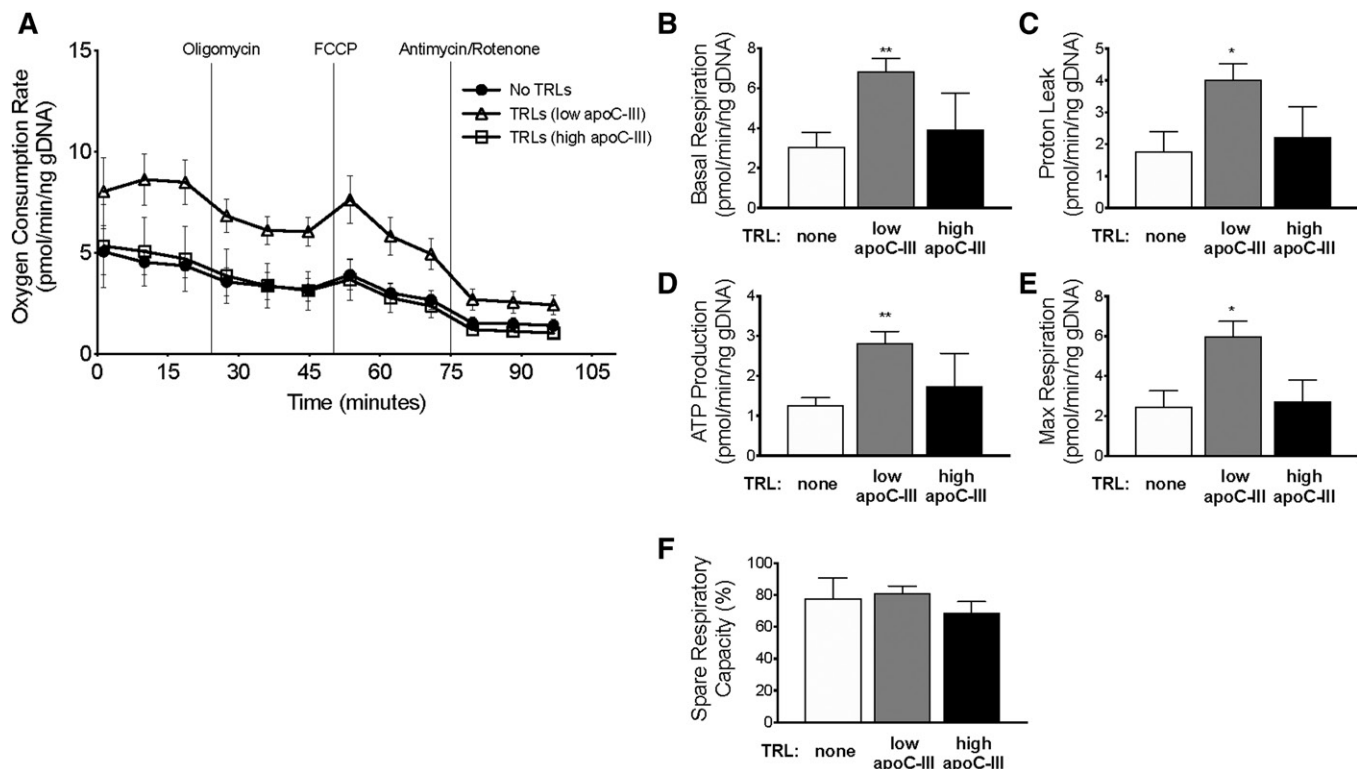


Fig. 6. Extracellular apoC-III inhibits the induction of mitochondrial respiration observed from basolateral TRL treatment. 3D WT enteroids were treated with TRLs containing low apoC-III content, high apoC-III content, or treated with PBS control. A: The following data were collected: OCR of WT enteroids under uninhibited conditions and in response to sequential treatment with oligomycin, FCCP, and antimycin/rotenone. Four biological replicates were used in OCR analysis. B–F: Analysis of MitoStress test showing changes in respiration, proton leak, ATP production, and percent spare respiratory capacity of WT enteroids in response to treatments. In all panels, error bars indicate SEM. Statistical significance and interaction between treatments was determined by two-tailed Student's *t*-test (**P* < 0.05, ***P* < 0.01).

FAO and TAG lipase gene expression is higher in *apoC-III*^{Tg} intestine during fasting

We found that *apoC-III*^{Tg} intestines have increased *CPT1B*, *ACOX1*, and *UCP2* mRNA expression in the fasting state compared with WT intestine (Fig. 4A), suggesting that *apoC-III*^{Tg} enterocytes have increased mitochondrial FAO during fasting conditions. Additionally, *ATGL* and *HSL* mRNA expression was significantly increased in fasted *apoC-III*^{Tg} intestine compared with WT (Fig. 4B). We confirmed that fasting *apoC-III*^{Tg} primary enterocytes contain less neutral lipid (via LipidTox Deep Red™ staining) than WT enterocytes (Fig. 4C). *APOC3* gene expression remains unchanged between WT and *apoC-III*^{Tg} intestine as well as between fasting and feeding conditions (Fig. 4D).

In WT intestine, *PGC1α*, *ATGL*, and *HSL* mRNA expression increases after an olive oil gavage compared with fasting expression levels (Figs. 3A, 4B). Interestingly, *PGC1α*, *ATGL*, and *HSL* are significantly downregulated in *apoC-III*^{Tg} intestine in response to an olive oil gavage compared with WT intestine (Figs. 3A, 4B). We hypothesize that the downregulation of *PGC1α*, *ATGL*, and *HSL* mRNA expression in fed *apoC-III*^{Tg} intestine is an attempt to conserve dietary lipid for chylomicron synthesis despite the increase in mitochondrial respiration (Fig. 3C, D). We conclude that mitochondrial FAO and TAG lipolysis are upregulated in *apoC-III*^{Tg} enterocytes during fasting conditions, and that

this could be explained by a loss of TAG substrates coming from the basolateral side.

High levels of plasma apoC-III inhibit intestinal uptake of TRLs

The intestine expresses LDLr, which functions in intestinal cholesterol uptake and transintestinal cholesterol excretion (TICE) (38). We hypothesized that high plasma apoC-III (Fig. 5A) inhibits intestinal uptake of TRLs in *apoC-III*^{Tg} mice. We confirmed that the intestine expresses high levels of *LDLR* at approximately one-third of liver expression (Fig. 5B) (15, 16). We measured mRNA expression of *LDLR* in intestines from WT and *apoC-III*^{Tg} mice during fasting and feeding conditions, and we confirmed that there is no significant change in *LDLR* expression due to apoC-III overexpression (Fig. 5C). Additionally, we found no significant changes in intestinal LDLr protein expression in WT and *apoC-III*^{Tg} mice (supplemental Fig. S1D). Intestinal *LDLR* mRNA expression is greater under fasting conditions compared with fed intestine (Fig. 5C). The intestine also expresses *VLDLR*, *LPL*, and *CD36*, which may contribute to an LDLr-independent pathway of uptake (Fig. 5D). Therefore, like other tissues that use TRLs, the intestine expresses TRL uptake machinery.

In vitro, apoC-III inhibits both LPL and LDLr, although the largest physiological effect of apoC-III is the inhibition

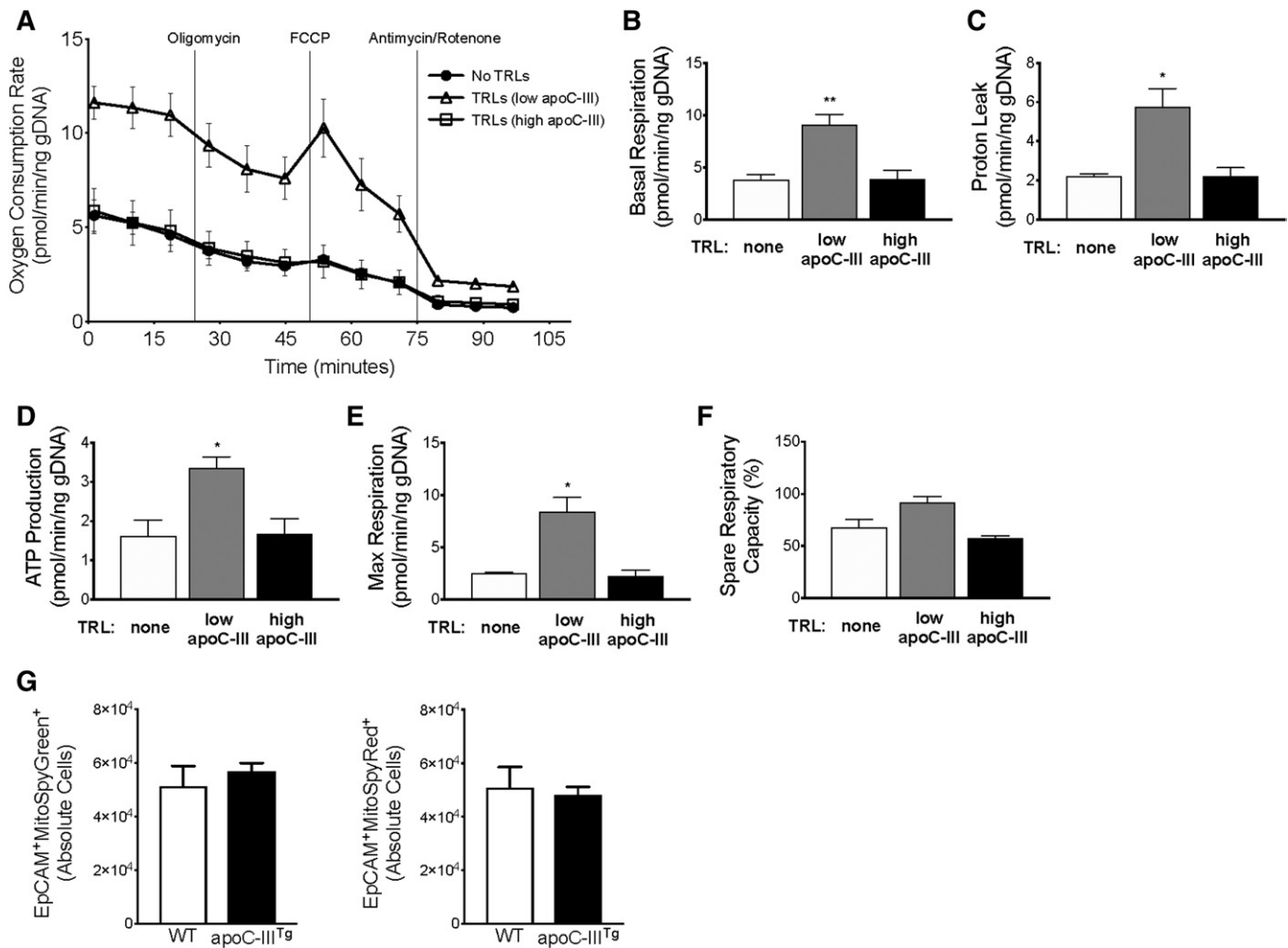


Fig. 7. Intracellular apoC-III overexpression does not regulate mitochondrial respiration. 3D *apoC-III*^{Tg} enteroids were treated with TRLs containing low apoC-III content, high apoC-III content, or treated with PBS control. **A:** The following data were collected: OCR of *apoC-III*^{Tg} enteroids under uninhibited conditions and in response to sequential treatment with oligomycin, FCCP, and antimycin/rotenone. Four biological replicates were used in OCR analysis. **B–F:** Analysis of MitoStress test showing changes in respiration, proton leak, ATP production, and percent spare respiratory capacity of *apoC-III*^{Tg} enteroids in response to treatments. Three biological replicates were used in OCR analysis. **G:** Mitochondrial content (MitoSpy GreenTM) and activity (MitoSpy RedTM) in untreated WT and *apoC-III*^{Tg} 3D enteroids measured by flow cytometry (n = 4–5 biological replicates per genotype). In all panels, error bars indicate SEM. Statistical significance and interaction between treatments was determined by two-tailed Student's *t*-test (**P* < 0.05, ***P* < 0.01).

of remnant clearance by LDLr in the liver (13). We treated WT 3D enteroids with VLDL (5 µg/ml DiI-labeled human VLDL), and we find that DiI uptake is dose-dependently decreased when recombinant human apoC-III protein is added to those VLDLs (Fig. 5E). These data are the first to show that excess apoC-III inhibits basolateral TRL uptake in the intestine.

Basolateral TRL treatment increases enterocyte basal respiration rate

We hypothesized that treatment of enterocytes with basolateral TRLs could provide an alternative non-dietary source of lipids for FAO in enterocytes. We measured the OCR in 3D WT enteroids treated with basolateral TRLs using Seahorse extracellular flux analysis (38). We isolated TRLs with low apoC-III content from WT mice to serve as a control to the TRLs with high apoC-III content (which were isolated from *apoC-III*^{Tg} mice). The TAG composition

of the TRLs varied between WT and *apoC-III*^{Tg} mice, so we normalized all TRL treatments to TAG concentration.

Treatment with TRLs containing low apoC-III content increased the basal respiration rate in WT enteroids compared with no TRL treatment (Fig. 6A, B). Both ATP production and proton leak are higher in cells treated with TRLs with low apoC-III relative to the no TRL control (Fig. 6C, D).

Maximal respiration is significantly increased in enteroids treated with TRLs containing low apoC-III compared with cells with no TRLs (Fig. 6E). It is worth noting that the response to the inhibitor FCCP is slightly blunted in enteroids compared with other cell types, and similar observations have been previously reported (37). We conclude that treatment with basolateral TRLs upregulates mitochondrial respiration and capacity in WT enteroids.

We next asked whether apoC-III could block the induction of mitochondrial respiration, presumably through

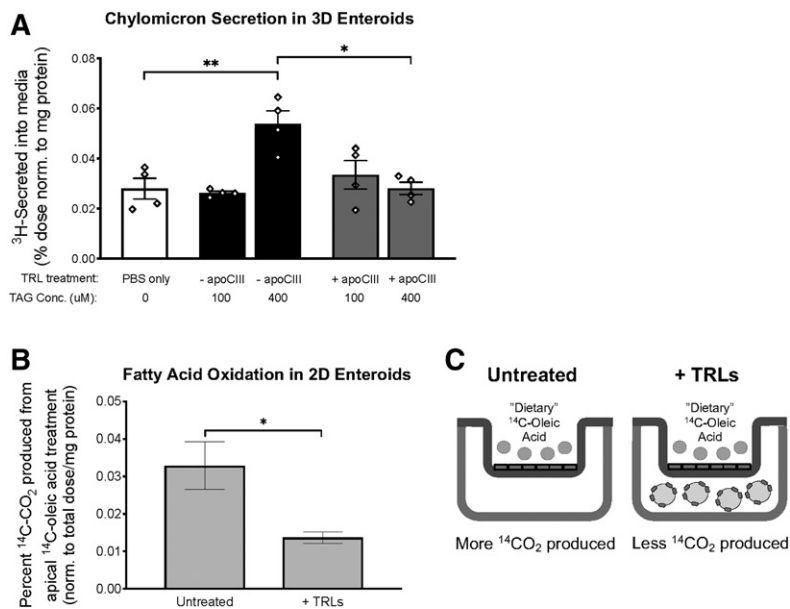


Fig. 8. Basolateral TRL uptake increases the secretion of dietary fat and decreases the oxidation of dietary FA. A: Chylomicron secretion was measured in 3D WT enteroids that were apically treated with lipid micelles containing ^3H -OA by measuring the amount of tritium (^3H) in the chase medium. 3D WT enteroids were treated with basolateral TRL at 100 and 400 μM final concentrations, and these TRLs either contained no apoC-III content ($-\text{apoC-III}$) or excess apoC-III ($+\text{apoC-III}$) on their surface. Statistical significance was determined using a one-way ANOVA with Tukey post hoc analysis ($*P < 0.05$, $**P < 0.01$, $***P < 0.0001$). B: FAO of dietary ^{14}C -OA was measured in 2D WT enteroids grown in a Transwell system treated with (+TRLs) and without (untreated) basolateral TRLs. C: Treatment conditions for FAO assay shown in panel B. Statistical significance and interaction between genotypes were determined by two-tailed Student's t -test ($*P < 0.05$, $**P < 0.01$).

inhibited TRL uptake. When 3D WT enteroids are treated with TRLs containing high apoC-III content, the cells respond similarly to cells that received no TRL treatment (Fig. 6). To further confirm the extrinsic role of apoC-III on enterocyte metabolism, we measured the OCR in *apoC-III*^{Tg} enteroids (Fig. 7A–F). We found that *apoC-III*^{Tg} enteroids behave similarly to WT enteroids during all treatments. Additionally, we measured mitochondrial mass and respiration in WT and *apoC-III*^{Tg} 3D enteroids using MitoSpy GreenTM and MitoSpy RedTM, respectively. We found that WT and *apoC-III*^{Tg} 3D enteroids have similar MitoSpy GreenTM and MitoSpy RedTM staining (Fig. 7G). We conclude that intracellular apoC-III overexpression does not regulate mitochondrial content or respiration, but basolateral TRLs and their apoC-III content modulate enterocyte mitochondrial respiration.

Our data showing a gradual decrease in OCR values and blunted OCR induction after FCCP injection match the findings from Fan et al. (37). Organoid cultures have previously been reported to have an anemic response to oligomycin and FCCP inhibitors, which differs significantly from more robust responses of crypt and stem cell cultures, as well as traditional 2D cell culture models. Like the Fan et al. (37) report, which showed the unique response of organoids to the inhibitors even though the organoids were 90% viable, our organoid cultures also have a blunted response to oligomycin and FCCP inhibitors. We confirmed by visual inspection before and after the Seahorse assay that the enteroids were intact and still maintaining 3D structure. We also added Y27623 Rho-kinase inhibitor compound (8) to inhibit apoptosis in response to the lack of Matrigel during the Seahorse assay (37).

BLST increases the secretion of dietary fat and decreases the oxidation of dietary FA

We treated 3D WT enteroids on the basolateral face with TRLs and measured chylomicron secretion using an apically delivered ^3H -OA tracer to determine whether basolateral TRL uptake can regulate the secretion of apical lipid.

When treated with 100 μM of TAG (in the form of TRLs), 3D enteroids secreted the same amount of apical ^3H compared with basolateral PBS treatment only (Fig. 8A). When treated with a higher concentration of TAG (400 μM), 3D enteroids were able to secrete twice as much ^3H to the basolateral medium (Fig. 8A). Additionally, when WT enteroids were treated with TRLs with high apoC-III content, there was no change in apical-to-basolateral ^3H secretion (Fig. 8A). We conclude that BLST preserves normal chylomicron secretion, and that the presence of excess apoC-III inhibits this effect.

We performed a radiolabeled FAO assay with 2D enteroids to determine whether BLST spares dietary lipids from FAO. 2D enteroids were cultured in Transwells and treated with apical ^{14}C -OA with and without TRLs in the basolateral chamber (a graphical summary of the treatment conditions and results from this experiment is shown in Fig. 8C). We find that enteroids exposed to basolateral TRLs convert twice as much apical ^{14}C -OA to $^{14}\text{CO}_2$ compared with enteroids that were not exposed to basolateral TRLs (Fig. 8B). We conclude that BLST provides fuel to enterocytes from TRLs, and that this fuel is used for mitochondrial oxidation. We hypothesize that in the absence of BLST (such as when apoC-III is high), enterocytes are denied this basolateral fuel and therefore use apical substrates.

DISCUSSION

In this study, we show that enterocytes take up TRLs on their basolateral surface, and that excess apoC-III on TRLs inhibits this uptake in a dose-dependent manner. We show that delivery of TRLs to the basolateral face of enterocytes stimulates enterocyte mitochondrial respiration, which suggests that TRLs may be a source of lipid substrates for enterocyte FAO. In vivo, *apoC-III*^{Tg} mice have a decrease in chylomicron secretion, and their enterocytes have a significant reduction in CLD size and number without any

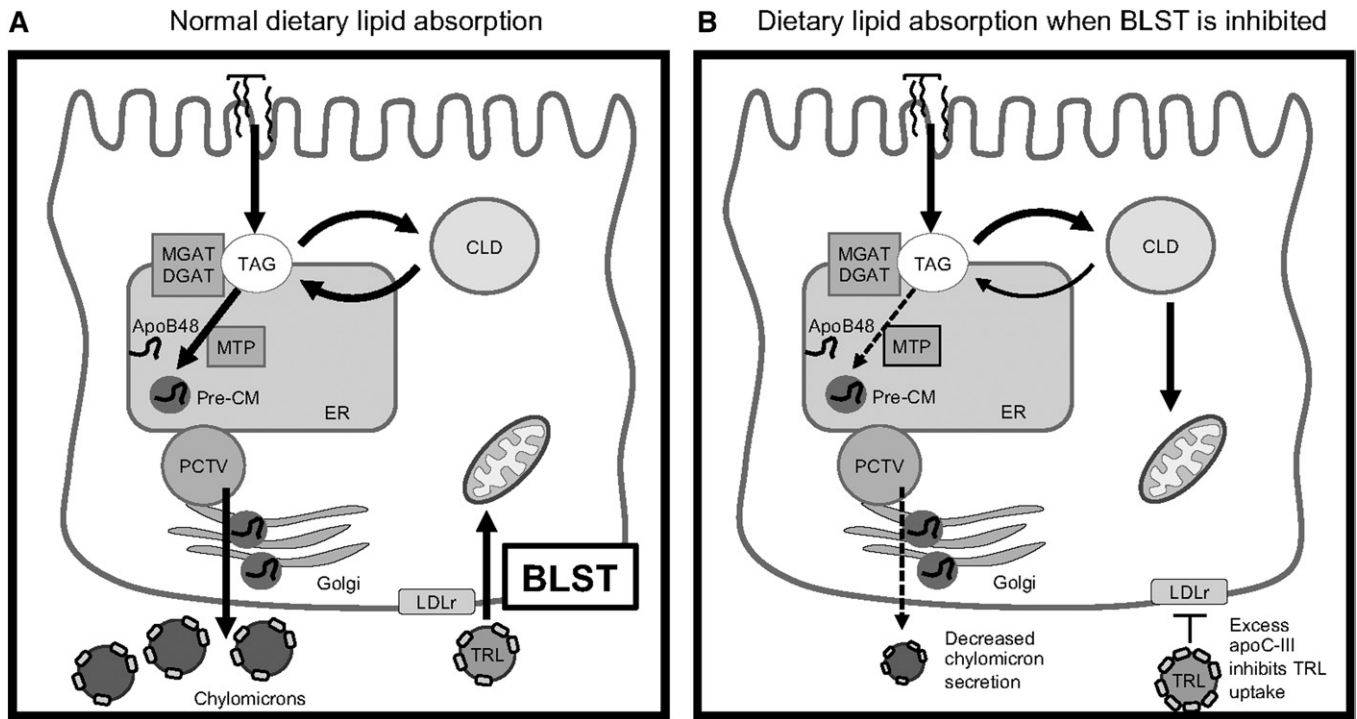


Fig. 9. Schematic diagram of the BLST pathway. A: Normal dietary lipid absorption where the majority of dietary lipid enters the chylomicron synthesis and secretion pathway, which is maintained by BLST providing TAG for mitochondrial FAO. B: Dietary lipid and CLD TAG are used for mitochondrial FAO when BLST is inhibited by excess apoC-III.

defects to apical lipid absorption or chylomicron synthetic machinery. We propose that excess plasma apoC-III decreases the availability of basolateral TRL fuel in *apoC-III^{Tg}* mice, and subsequently promotes the oxidation of dietary FAs, which reduces the lipid pool for the chylomicron secretion pathway.

Under normal circumstances, the majority of dietary TAG that is stored in CLDs is saved for chylomicron synthesis and spared from mitochondrial FAO in the enterocyte. CLD structural proteins and lipases are known to regulate the availability of TAG to the chylomicron synthesis pathway (33, 34, 39, 40). Although the relationship between CLD mRNA and protein expression has not been confirmed, we used mRNA abundance as a marker to detect major changes in the lipid metabolic pathways involving CLDs in the intestine (6, 33, 34). The changes to mRNA expression are consistent with our proposed mechanism that there is a BLST pathway that provides lipid substrates to enterocytes, and that TAG substrate from the diet and/or CLDs makes up for the loss of these basolateral substrates if necessary (schematic diagram of BLST provided in Fig. 9). The result of inhibited BLST is a decrease in chylomicron TAG secretion, a reduction in CLD size and number, and an increase in intracellular lipid hydrolysis.

It has been previously shown that enterocytes transport circulating albumin-bound FFAs across their basolateral membrane, and that these FFAs are primarily used for esterification of phospholipids, membrane biogenesis, and FAO (41–43). We propose that TRL uptake provides TAG substrates for the enterocyte, thus preserving dietary lipids


for chylomicron synthesis. Our data suggest that the role of apoC-III in this process is solely extracellular; we show that OCR is induced in WT enteroids that were treated with TRLs, and that the OCR induction is blunted when WT enteroids were treated with TRLs that contain high apoC-III content. When comparing the OCR in untreated WT and *apoC-III^{Tg}* 3D enteroids, we find that both WT and *apoC-III^{Tg}* 3D enteroids have similar OCR responses.

Intestinal energy metabolism is complex because the energy source for the intestinal mucosa is a mixture of arterial and luminal substrates. In the fed state, the intestine primarily relies on dietary amino acids for fuel (and specifically dietary glutamate and aspartate) (44). In the fasting state, the intestine gets ~84% of its total energy from arterial glucose, glutamine, and glutamate (44–46). In both physiologic states, FFAs are available, either from dietary lipids at the apical membrane or from plasma TRLs and FFAs at the basolateral membrane. Our data suggest that the loss of the basolateral TRL fuel source (when apoC-III inhibits basolateral LDLr) has a significant impact on enterocyte lipid metabolism that results in decreased chylomicron TAG secretion.

A fundamental question that our study proposes is whether this is physiologically important when human plasma levels of apoC-III are never as extreme as the levels achieved in our *apoC-III^{Tg}* mouse model. However, there are many clinical situations when humans do have elevations in plasma apoC-III, including human apoC-III polymorphisms, hyperlipidemia, and TRL clearance defects (47). The clinical importance of high levels of apoC-III is also evidenced by the multiple pharmaceutical

approaches that are now being developed to treat patients with high apoC-III levels, including apoC-III antisense (48) and antibody drugs (49). If human intestine responds to the inhibition of BLST as our mouse enteroids do, then the human intestine may secrete smaller and potentially pro-atherogenic lipoproteins during dietary lipid absorption.

We conclude that these data are the first to show that enterocytes take up TRLs on the basolateral face, that excess apoC-III decreases TRL uptake, and that this regulates chylomicron secretion and enterocyte metabolism. This BLST pathway shares elements of the previously described TICE pathway (50), which transports LDL- and HDL-cholesterol from the basolateral face to the intestinal lumen. Studies of TICE have not previously determined the transport of TAG or the impact of TICE on enterocyte metabolism (37, 51). We propose that BLST likely shares lipid receptors (i.e., LDLr) with TICE, but the BLST pathway also has key features that are not shared with TICE. These include: 1) the use of TRL substrates; 2) the impact of those substrates of mitochondrial oxidation; and 3) chylomicron secretion.

Therefore, our studies suggest that TICE is no longer the only lipid transport pathway taking place on the basolateral side of the enterocyte; we propose that the pathway we describe here (BLST) is occurring (possibly subclinically) under normal circumstances (where most enterocyte energy needs are being met with amino acids), but that under conditions of metabolic dysfunction and altered plasma lipids, the loss of this pathway may be critical in changing the lipoprotein output of the enterocyte. 

This work was performed in part at the Biosciences Electron Microscopy Facility of the University of Connecticut and the University of Cincinnati Medical Center. Mouse Metabolic Phenotyping Center is supported by U24 DK059630.

REFERENCES

- Hogue, J. C., B. Lamarche, A. J. Tremblay, J. Bergeron, C. Gagné, and P. Couture. 2007. Evidence of increased secretion of apolipoprotein B-48-containing lipoproteins in subjects with type 2 diabetes. *J. Lipid Res.* **48**: 1336–1342.
- Wong, A. T. Y., D. C. Chan, J. Pang, G. F. Watts, and P. H. R. Barrett. 2014. Plasma apolipoprotein B-48 transport in obese men: A new tracer kinetic study in the postprandial state. *J. Clin. Endocrinol. Metab.* **99**: E122–E126.
- Wang, Y., S. Ghoshal, M. Ward, W. J. S. de Villiers, J. Woodward, and E. Eckhardt. 2009. Chylomicrons promote intestinal absorption and systemic dissemination of dietary antigen (ovalbumin) in mice. *PLoS One.* **4**: e8442.
- Laugerette, F., C. Vors, N. Peretti, and M-C. C. Michalski. 2011. Complex links between dietary lipids, endogenous endotoxins and metabolic inflammation. *Biochimie.* **93**: 39–45.
- Higgins, V., and K. Adeli. 2017. Postprandial dyslipidemia: pathophysiology and cardiovascular disease risk assessment. *EJIFCC.* **28**: 168–184.
- D'Aquila, T., D. Sirohi, J. M. Grabowski, V. E. Hedrick, L. N. Paul, A. S. Greenberg, R. J. Kuhn, and K. K. Buhman. 2015. Characterization of the proteome of cytoplasmic lipid droplets in mouse enterocytes after a dietary fat challenge. *PLoS One.* **10**: e0126823.
- Beilstein, F., V. Carrière, A. Leturque, and S. Demignot. 2016. Characteristics and functions of lipid droplets and associated proteins in enterocytes. *Exp. Cell Res.* **340**: 172–179.
- Xiao, C., S. Dash, C. Morgantini, and G. F. Lewis. 2016. Intravenous glucose acutely stimulates intestinal lipoprotein secretion in healthy humans. *Arterioscler. Thromb. Vasc. Biol.* **36**: 1457–1463.
- Reeds, P. J., D. G. Burrin, B. Stoll, and F. Jahoor. 2000. Intestinal glutamate metabolism. *J. Nutr.* **130**: 978S–982S.
- Windmueller, H. G., and A. E. Spaeth. 1978. Identification of ketone bodies and glutamine as the major respiratory fuels in vivo for postabsorptive rat small intestine. *J. Biol. Chem.* **253**: 69–76.
- Wang, F., A. B. Kohan, H. Henry Dong, Q. Yang, M. Xu, S. Huesman, D. Lou, D. Y. Hui, and P. Tso. 2014. Overexpression of apolipoprotein C-III decreases secretion of dietary triglyceride into lymph. *Physiol. Rep.* **2**: e00247.
- Jattan, J., C. Rodia, D. Li, A. Diakhate, H. Dong, A. Bataille, N. F. Shroyer, and A. B. Kohan. 2017. Using primary intestinal enteroids to study dietary TAG absorption, lipoprotein synthesis, and the role of apoC-III in the intestine. *J. Lipid Res.* **58**: 853–865.
- Gordts, P. L. S. M., R. Nock, N-H. Son, B. Ramms, I. Lew, J. C. Gonzales, B. E. Thacker, D. Basu, R. G. Lee, A. E. Mullick, et al. 2016. ApoC-III inhibits clearance of triglyceride-rich lipoproteins through LDL family receptors. *J. Clin. Invest.* **126**: 2855–2866.
- Khetarpal, S. A., A. Qamar, J. S. Millar, and D. J. Rader. 2016. Targeting ApoC-III to reduce coronary disease risk. *Curr. Atheroscler. Rep.* **18**: 54.
- Fong, L. G., E. Bonney, J. C. Kosek, and A. D. Cooper. 1989. Immunohistochemical localization of low density lipoprotein receptors in adrenal gland, liver, and intestine. *J. Clin. Invest.* **84**: 847–856.
- Sviridov, D., J. M. Hoeg, T. Eggerman, S. J. Demosky, I. G. Safonova, and H. B. Brewer. 2003. Low-density lipoprotein receptor and apolipoprotein A-I and B expression in human enterocytes. *Digestion.* **67**: 67–70.
- Le May, C., J. M. Berger, A. Lespine, B. Pillot, X. Prieur, E. Letessier, M. M. Hussain, X. Collet, B. Cariou, and P. Costet. 2013. Transintestinal cholesterol excretion is an active metabolic process modulated by PCSK9 and statin involving ABCB1. *Arterioscler. Thromb. Vasc. Biol.* **33**: 1484–1493.
- Ito, Y., N. Azrolan, A. O'Connell, A. Walsh, and J. L. Breslow. 1990. Hypertriglyceridemia as a result of human apo CIII gene expression in transgenic mice. *Science.* **249**: 790–793.
- Aalto-Setälä, K., E. A. Fisher, X. Chen, T. Chajek-Shaul, T. Hayek, R. Zechner, A. Walsh, R. Ramakrishnan, H. N. Ginsberg, and J. L. Breslow. 1992. Mechanism of hypertriglyceridemia in human apolipoprotein (apo) CIII transgenic mice. Diminished very low density lipoprotein fractional catabolic rate associated with increased apo CIII and reduced apo E on the particles. *J. Clin. Invest.* **90**: 1889–1900.
- Folch, J., M. Lees, and G. H. Sloane Stanl. 1957. A simple method for the isolation and purification of total lipides from animal tissues. *J. Biol. Chem.* **226**: 497–509.
- Soayfane, Z., F. Tercé, M. Cantiello, H. Robenek, M. Nauze, V. Bézirard, S. Allart, B. Payré, F. Capilla, C. Cartier, et al. 2016. Exposure to dietary lipid leads to rapid production of cytosolic lipid droplets near the brush border membrane. *Nutr. Metab. (Lond.)* **13**: 48.
- Li, D., H. Dong, and A. B. Kohan. 2017. The isolation, culture, and propagation of murine intestinal enteroids for the study of dietary lipid metabolism. *In* Methods in Molecular Biology. Humana Press, New York. 1–10.
- Garcia-Bermudez, J., L. Baudrier, E. C. Bayraktar, Y. Shen, K. La, R. Guarecupo, B. Yucel, D. Fiore, B. Tavora, E. Freinkman, et al. 2019. Squalene accumulation in cholesterol auxotrophic lymphomas prevents oxidative cell death. *Nature.* **567**: 118–122.
- Chan, D. C., G. F. Watts, M. N. Nguyen, and P. H. R. Barrett. 2006. Apolipoproteins C-III and A-V as predictors of very-low-density lipoprotein triglyceride and apolipoprotein B-100 kinetics. *Arterioscler. Thromb. Vasc. Biol.* **26**: 590–596.
- Wang, Y., M. DiSalvo, D. B. Gunasekara, J. Dutton, A. Proctor, M. S. Lebhar, I. A. Williamson, J. Speer, R. L. Howard, N. M. Smiddy, et al. 2017. Self-renewing monolayer of primary colonic or rectal epithelial cells. *Cell. Mol. Gastroenterol. Hepatol.* **4**: 165–182.e7.
- Srinivasan, B., A. R. Kolli, M. B. Esch, H. E. Abaci, M. L. Shuler, and J. J. Hickman. 2015. TEER measurement techniques for in vitro barrier model systems. *J. Lab. Autom.* **20**: 107–126.
- Conlon, D. M., T. Thomas, T. Fedotova, A. Hernandez-Ono, G. Di Paolo, R. B. Chan, K. Ruggles, S. Gibeley, J. Liu, and H. N. Ginsberg. 2016. Inhibition of apolipoprotein B synthesis stimulates endoplasmic reticulum autophagy that prevents steatosis. *J. Clin. Invest.* **126**: 3852–3867.

28. Jandacek, R. J., J. E. Heubi, and P. Tso. 2004. A novel, noninvasive method for the measurement of intestinal fat absorption. *Gastroenterology*. **127**: 139–144.
29. Xie, Y., E. P. Newberry, S. G. Young, S. Robine, R. L. Hamilton, J. S. Wong, J. Luo, S. Kennedy, and N. O. Davidson. 2006. Compensatory increase in hepatic lipogenesis in mice with conditional intestine-specific Mttp deficiency. *J. Biol. Chem.* **281**: 4075–4086.
30. Yen, C.-L. E., D. W. Nelson, and M.-I. Yen. 2015. Intestinal triacylglycerol synthesis in fat absorption and systemic energy metabolism. *J. Lipid Res.* **56**: 489–501.
31. Obrowsky, S., P. G. Chandak, J. V. Patankar, S. Povoden, S. Schlager, E. E. Kershaw, J. G. Bogner-Strauss, G. Hoefler, S. Levak-Frank, and D. Kratky. 2013. Adipose triglyceride lipase is a TG hydrolase of the small intestine and regulates intestinal PPAR α signaling. *J. Lipid Res.* **54**: 425–435.
32. Gao, Y., D. W. Nelson, T. Banh, M.-I. Yen, and C.-L. E. Yen. 2013. Intestine-specific expression of MOGAT2 partially restores metabolic efficiency in Mogat2-deficient mice. *J. Lipid Res.* **54**: 1644–1652.
33. Zhang, L.-J., C. Wang, Y. Yuan, H. Wang, J. Wu, F. Liu, L. Li, X. Gao, Y.-L. Zhao, P.-Z. Hu, et al. 2014. Cideb facilitates the lipidation of chylomicrons in the small intestine. *J. Lipid Res.* **55**: 1279–1287.
34. Frank, D. N., E. S. Bales, J. Monks, M. J. Jackman, P. S. MacLean, D. Ir, C. E. Robertson, D. J. Orlicky, and J. L. McManaman. 2015. Perilipin-2 modulates lipid absorption and microbiome responses in the mouse intestine. *PLoS One*. **10**: e0131944.
35. Scarpulla, R. C. 2011. Metabolic control of mitochondrial biogenesis through the PGC-1 family regulatory network. *Biochim. Biophys. Acta*. **1813**: 1269–1278.
36. Fernandez-Marcos, P. J., and J. Auwerx. 2011. Regulation of PGC-1 α , a nodal regulator of mitochondrial biogenesis. *Am. J. Clin. Nutr.* **93**: 884S–890.
37. Jakulj, L., T. H. van Dijk, J. F. de Boer, R. S. Kootte, M. Schonewille, Y. Paalvast, T. Boer, V. W. Bloks, R. Boverhof, M. Nieuwdorp, et al. 2016. Transintestinal cholesterol transport is active in mice and humans and controls ezetimibe-induced fecal neutral sterol excretion. *Cell Metab.* **24**: 783–794.
38. Fan, Y. Y., L. A. Davidson, E. S. Callaway, G. A. Wright, S. Safe, and R. S. Chapkin. 2015. A bioassay to measure energy metabolism in mouse colonic crypts, organoids, and sorted stem cells. *Am. J. Physiol. Gastrointest. Liver Physiol.* **309**: G1–G9.
39. Bas, T., and L. H. Augenlicht. 2014. Real time analysis of metabolic profile in ex vivo mouse intestinal crypt organoid cultures. *J. Vis. Exp.* **93**: e52026.
40. Xie, P., F. Guo, Y. Ma, H. Zhu, F. Wang, B. Xue, H. Shi, J. Yang, and L. Yu. 2014. Intestinal Cgi-58 deficiency reduces postprandial lipid absorption. *PLoS One*. **9**: e91652.
41. Shiau, Y.-F. F., D. A. Popper, M. Reed, C.-E. Umstetter, D. Capuzzi, and G. M. Levine. 1985. Intestinal triglycerides are derived from both endogenous and exogenous sources. *Am. J. Physiol.* **248**: G164–G169.
42. Mansbach, C. M., and R. F. Dowell. 1992. Uptake and metabolism of circulating fatty acids by rat intestine. *Am. J. Physiol.* **263**: G927–G933.
43. Storch, J., Y. X. Zhou, and W. S. Lagakos. 2008. Metabolism of apical versus basolateral sn-2- monoacylglycerol and fatty acids in rodent small intestine. *J. Lipid Res.* **49**: 1762–1769.
44. Windmueller, H. G., and A. E. Spaeth. 1976. Metabolism of absorbed aspartate, asparagine, and arginine by rat small intestine in vivo. *Arch. Biochem. Biophys.* **175**: 670–676.
45. Van Der Schoor, S. R., P. J. Reeds, B. Stoll, J. F. Henry, J. R. Rosenberger, D. G. Burrin, and J. B. Van Goudoever. 2002. The high metabolic cost of a functional gut. *Gastroenterology*. **123**: 1931–1940.
46. Stoll, B., D. G. Burrin, J. Henry, H. Yu, F. Jahoor, and P. J. Reeds. 1999. Substrate oxidation by the portal drained viscera of fed piglets. *Am. J. Physiol.* **277**: E168–E175.
47. Rammes, B., and P. L. S. M. Gordts. 2018. Apolipoprotein C-III in triglyceride-rich lipoprotein metabolism. *Curr. Opin. Lipidol.* **29**: 171–179.
48. Gaudet, D., V. J. Alexander, B. F. Baker, D. Brisson, K. Tremblay, W. Singleton, R. S. Geary, S. G. Hughes, N. J. Viney, M. J. Graham, et al. 2015. Antisense inhibition of apolipoprotein C-III in patients with hypertriglyceridemia. *N. Engl. J. Med.* **373**: 438–447.
49. Khetarpal, S. A., X. Zeng, J. S. Millar, C. Vitali, A. V. H. Somasundara, P. Zannoni, J. A. Landro, N. Barucci, W. J. Zavadski, Z. Sun, et al. 2017. A human APOC3 missense variant and monoclonal antibody accelerate apoC-III clearance and lower triglyceride-rich lipoprotein levels. *Nat. Med.* **23**: 1086–1094.
50. van der Velde, A. E., G. Brufau, and A. K. Groen. 2010. Transintestinal cholesterol efflux. *Curr. Opin. Lipidol.* **21**: 167–171.
51. Temel, R. E., and J. M. Brown. 2015. A new model of reverse cholesterol transport: EnTICEing strategies to stimulate intestinal cholesterol excretion. *Trends Pharmacol. Sci.* **36**: 440–451.
52. D'Aquila, T., Y. H. Hung, A. Carreiro, and K. K. Buhman. 2016. Recent discoveries on absorption of dietary fat: Presence, synthesis, and metabolism of cytoplasmic lipid droplets within enterocytes. *Biochim. Biophys. Acta*. **1861**: 730–747.
53. Hung, Y. H., A. L. Carreiro, and K. K. Buhman. 2017. Dgat1 and Dgat2 regulate enterocyte triacylglycerol distribution and alter proteins associated with cytoplasmic lipid droplets in response to dietary fat. *Biochim. Biophys. Acta Mol. Cell Biol. Lipids*. **1862**: 600–614.